The mechanical properties of lipid nanoparticles depend on the type of biomacromolecule they are loaded with

Sixtine de Chateauneuf Randon, Bruno Bresson, Manon Ripoll, Sylvain Huille, Etienne Barthel, Cecile Monteux

The mechanical properties of lipid nanoparticles depend on the type of biomacromolecule they are loaded with

Sixtine de Chateauneuf Randon,[†] Bruno Bresson,[*,†] Manon Ripoll,[*,‡] Sylvain Huille,[*,¶] Etienne Barthel,[†] and Cécile Monteux[*,†]

†*Laboratoire Sciences et Ingénierie de la Matière Molle, CNRS UMR 7615, PSL University, Sorbonne University, ESPCI Paris, 10 rue Vauquelin, Cedex 05 75231 Paris, France*

‡*Sanofi Pasteur, 1541 av Marcel Mérieux, 69280 Marcy l'Etoile*

¶*Sanofi R&D, Impasse Des Ateliers, 94400 Vitry-sur-Seine, France*

E-mail: bruno.bresson@espci.fr; Manon.Ripoll@sanofi.com; Sylvain.Huille@sanofi.com; cecile.monteux@espci.fr

Abstract

For drug delivery systems the mechanical properties of the drug carriers are suspected to play a crucial role in the delivery process. However there is a lack of reliable methods available to measure the mechanical properties of drug carriers which hampers the establishment of a link between delivery efficiency and mechanical parperties of carriers. Lipid nanoparticles (LNPs) are advanced systems for delivering nucleic acids to target cell populations for vaccination purposes (mRNA) or the development of new drugs. Hence it is crucial to develop reliable techniques to measure the mechanical properties of LNPs. In this article, we use AFM to image and probe the mechanical properties of LNP which are either loaded with two different biopolymers either pDNA or mRNA. Imaging the LNP before and after the indentation as well as recording the retraction curve enables us to obtain more insight on

how the AFM tip penetrates into the particle and to determine whether the deformation of the LNP is reversible. For pDNA, the indentation by the tip leads to the irreversible rupture of the LNPS while the deformation is reversible for the mRNA-loaded LNPs. Moreover, the forces reached for pDNA are higher than for mRNA. These results paves the way toward the establishment of the link between the LNP formulation and the delivery efficiency.

Introduction

Lipid nanoparticles (LNPs) are the best-known advanced systems for delivering nucleic acids to target cell populations for vaccination purposes (mRNA)[1–3] or for the development of new drugs (mRNA, siRNA, microRNA...). LNP are first taken up by the cell via endocytosis and then can release their nucleic acid cargo into the cell cytoplasm; in the case of mRNA, the delivery takes place in the cytosol and in the case of DNA an additional diffusion barrier must be considered up to the nucleus of the cell for transcription. Despite the amazing progress achieved by fine-tuned ionizable lipids depending on the pH within extra and intracellular compartments[4] LNPs still suffer from poor efficiency resulting in a small fraction of the nucleic acid cargo being delivered properly for transfection. LNPs remain often trapped in endosomal compartments where they degrade through the endosome-lysosome pathway which limits the delivery by a poor endosomal escape of the nucleic acid. Nanoparticles can also enter the cell differently depending on their particular size, shape, or mechanical properties[5–7]. The composition of LNPs controls their structure and stability[2,3,8,9]. The ionizable lipids complex with the negatively charged mRNA, while pegylated lipids stabilize sterically the LNP against aggregation and flocculation. Cholesterol is usually added to provide increased stability. Characterizing these LNP is crucial both for quality control and for optimization of their formulation and efficiency[1,10–14]. Characterization methods include size measurements using Dynamic light scattering DLS[11,12] or observation of their shape and internal structure with cryoTEM[13,15]. CryoTEM measurements have evidenced that LNPs contain several aqueous compartments whose number and spatial arrangements depend on the formulation[13]. Other valuable information can be obtained such as their zeta potential or melting temperature using Dynamic Scanning calorimetry while small angle X-

ray scattering allows the determination of their structure factor[13]. Stiffness which can alter the cellular uptake appears as an important feature for biology and the relationship between particle mechanical properties and drug delivery processes has been suggested as an appealing way by tuning the stiffness of particles to improve therapeutic efficiency[16–20]. Atomic force microscopy, which enables to probe the interaction between a nanometric tip and a surface is a powerful tool to obtain both images and mechanical properties of soft nanoparticles. One challenge that one faces when using AFM to characterize phospholipid-based nanoparticles in situ in a liquid medium is to immobilize the particles on a substrate. Indeed drying soft nanoparticles on a surface such as LNP results in structural damage to the particles' lipid membrane[21–23]. Several studies which focused on the in situ imaging of vesicles on a substrate[24–28] such as Reviakin and Brisson[24] Jaas[25], Richter[27,28] showed that the vesicles tend to destabilize into bilayers when the interaction between the vesicles and the substrate is strong. On the opposite, when the vesicles are repelled by the surface or when the interactions are weak the particles do not adsorb on the substrate and hence cannot be imaged. Recently LNP were successfully immobilized and imaged on a solid surface in a liquid medium using antiPEG coating on a glass surface[29]. When turning to mechanical measurements of delivery vehicles by AFM very little literature is available and mostly concerns polymer capsules[30–33] for which force-indentation curves were measured to obtain the stiffness of capsules of varying sizes and shell thicknesses. From these curves, one can deduce an effective Young modulus of the capsules using the Reissner model, which is valid when the thickness of the shell is much lower than the particle size. The deformation of nanometric model liposomes using AFM was performed in references[34,35] where the Reissner model was used to deduce the Young modulus of the liposomes as well as the bending rigidity of the phospholipidic membranes. In the case of multilamellar liposomes the measured stiffness increases with the number of lamellas[36]. However, the structure of LNP seems to be more disordered than the one of standard liposomes[37] which complicates the quantitative analysis of AFM results to obtain a value for an elastic modulus[38]. In this article we use AFM to image and probe the mechanical properties of LNP whose content is varied as they are loaded either with pDNA a rigid polymer or mRNA which is a more flexible polymer. Imaging the LNP before and after the indentation as well as recording the retraction curve enables us to obtain more insight on how

the AFM tip penetrates into the particle and to determine whether the deformation of the LNP is reversible. During the retraction of the tip we measure large adhesion forces which are probably due to the penetration of the tip inside the LNP and to the establishment of a capillary bridge between the tip and the LNP. After the retraction, the LNP loaded with pDNA are irreversibly destroyed while those containing mRNA tend to heal after indentation. By providing a method to measure the mechanical properties of LNP our study is a first step that paves the way toward the establishment of the link between mechanical properties of LNP and their delivery efficiency.

Experimental section

Lipid nanoparticles (LNP)

Products

1,2-dioleoyl-sn-glycero-3-phosphocholine (DOPC), 1,2-dimyristoyl-rac-glycero-3-methoxy-polyethylene glycol-2000 (DMG-PEG2000), and cholesterol (plant-derived) were purchased from Avanti Polar Lipids (Alabaster, AL, USA). The ionizable lipid, 4-(dimethylamino)-butanoic acid, (10Z,13Z)-1-(9Z,12Z)-9,12-octadecadien-1-yl-10,13-nonadecadien-1-yl ester (Dlin-MC3-DMA, henceforth termed MC3), was obtained from SAI Life Science (Hyderabad, India). Citric acid, sodium citrate tribasic dehydrate, and Triton x100 were acquired from Sigma–Aldrich (France). Phosphate-buffered saline 10X (PBS, pH 7.4) was obtained from Thermo Fisher Scientific (France). The gWiz-GFP plasmid was purchased from Aldevron (North Dakota, USA), and the mRNA-Luc from Trilink (California, USA).

Formulation

Lipids were solubilized in ethanol at 20 mg/mL at molar ratios of 50:10:38.5:1.5 (ionizable lipid/Phospholipid/cholesterol/PEGLipid). pDNA or mRNA were mixed with 50 mM citrate buffer at $pH = 4$. The selected lipid/mRNA concentrations yielded a constant N/P ratio of 6 (cationic nitrogen groups from the ionizable lipid over anionic phosphate groups from the mRNA). The ethanolic and the aqueous phases were then injected into the NanoAssemblr™

Benchtop microfluidic mixer using NxGen microfluidic cartridge (Precision Nanosystems, Vancouver, BC) at a flow rate ratio of 1:3 with a combined final flow rate of 4 mL/min. These flow rate and ratios conditions were chosen based on previous publications of Ripoll et al.[39] and Sabnis et al.[40]. Ethanol was then removed and the citrate buffer was replaced by PBS 1X using Amicon Ultra Centrifugal Filters (EMD Millipore, Billerica, MA) so that the final pH of the LNP solution is $pH = 7.4$. The formulations were finally passed through a 0.22 µm filter and stored liquid at $4°C$ under nitrogen atmosphere. We note that for all experiments we start with a LNP solution initially at $pH = 7.4$ in a PBS buffer. In the case where the experiments are performed at $pH = 4$, the pH is reduced from $pH = 7.4$ to $pH = 4$ by adding citrate acid into the solution.

Characterization

Measurements of nanoparticle size and polydispersity

The particle size and the polydispersity index (PDI) were measured by dynamic light scattering using a Malvern Zetasizer NanoZS (Worcestershire, UK). LNPs were diluted 100 times in PBS and added to a μ-cuvette. The dispersant (PBS) refractive index (RI) and viscosity values were 1.34 and 1.02 cP, respectively, whereas the material RI was 1.45. As can be seen in Figure SI, LNPs diameter is of the order of 100 nm.

Quantification of nucleic acid loading

The pDNA encapsulation efficiency was determined using the PicoGreen DNA assay (Life Technologies, Burlington, ON) whereas the mRNA encapsulation efficiency was determined using the Ribogreen assay (Life Technologies, Burlington, ON). Briefly, 100 µL of the diluted fluorescent dye was added to 100 µL of diluted LNPs in the presence or absence of 1%(w/v) Triton-X100 in TE buffer and incubated in the absence of light for 5 min. Nucleic acids were quantified by measuring fluorescence (ex/em = 480 nm/520 nm) using a fluorimeter (Varioskan Lux Microplate reader, Thermo Fisher). A linear calibration curve up to 1000 ng/mL was performed using the standard DNA or RNA sample provided in the kit.

The encapsulation ratio was calculated by the following formula:

$$EE(\%) = \frac{1 - nucleic\ acid\ concentration\ in\ absence\ of\ Triton}{nucleic\ acid\ in\ presence\ of\ Triton} \times 100$$

Atomic Force Microscope (AFM)

Substrate preparation

Two different types of substrates were used. We first use a mica sheet cleaved with an adhesive tape. Second, we use glass slides washed using cerium oxide powder (Cerox^{TM}, Solvay) to activate the hydroxyl groups on the surface and trigger hydrogen bonds with the PEG groups of the LNPs. This in-house protocol involves depositing a drop of solution containing the Cerox^{TM} powder at $10\%wt$ on the glass surface and rubbing the Cerox^{TM} solution against the glass surface with a humidified sponge for one minute and then rinsing with deionized water for several minutes to remove the Cerox^{TM} powder. This protocol enables perfect wetting between the glass surface and water due to the reduction of silicon oxide groups into silicon hydroxyl groups.

Imaging protocol

A drop of the LNP solution at a concentration of $5.10^{-1}\%wt$ is deposited on the solid substrate and the AFM analysis is performed by imaging the particles that adsorb on the substrate in the liquid medium (Dimension Icon with Scan Asyst). The results are analyzed using the NanoScopeAnalysis software and a MatLab script. Two types of BRUKER silicon tips were used, either a SCANASYST-FLUID+ tip (stiffness: 0.7 N/m, diameter: 4 nm), or a MLCT tip (stiffness: 0.03 N/m, diameter: 40 nm). The imaging mode used is the PeakForce Quantitative Nanomechanics (QNM) performed at a scan rate of 1 kHz using an applied force below 100 pN and an amplitude of 50 nm to avoid the deformation of the LNP by the tip. The images are taken with a width/height ratio of 2, 256 points per line, and 128 lines. The images are flattened before analysis. The stiffness of each tip is measured by recording an approach retract curve on the substrate. The slope of the obtained force-distance curve corresponds to the tip stiffness.

Protocol to obtain the mechanical properties

To determine how reversibly the particles are deformed during the indentation measurements we choose to image the particles before and after the mechanical measurements. The

particles are first imaged in peakforce using the protocol described above with an MLCT tip (stiffness: 0.03 N/m, diameter: 40 nm). Second, we record three successive force-distance curves at 1 Hz on the center of one particle; we eventually repeat this step with 2 to 4 other particles. Third, we re-image the particles to determine how the particles have been deformed.

The baselines of the force curves are straightened and set to zero. In addition, the results are sorted to select baselines that do not oscillate. For visibility reasons, the baselines ($h = 0$) are cut off in the figures shown. $h = 0$ corresponds to contact between the tip with the surface. The zero point is set when the curve differs from the baseline.

We note that the local concentration of LNP on the surface varies, from densely packed to isolated, by investigating different areas inside the water drop. All the measurements presented in the main text of this article are performed in zones of the drops where the LNPs are densely packed to avoid any rearrangement of the particles on the surface during the indention. This protocol enables us to obtain a reliable forcing of the LNP and to differentiate the pDNA and mRNA LNPs. In the SI we show results obtained in zones where the pDNA LNP are isolated.

Results and discussion

Stability of the LNP during AFM imaging

Imaging and probing the mechanical properties of LNP with AFM in water requires fixing the particles on a solid surface. Although mica is often used as a substrate to perform AFM measurements we find that the LNP cannot be imaged at pH = 7.4 on mica because of a lack of attractive interactions between the LNP and the mica surface, consistently with Takeshi et al[29]. Using the fact that one of the lipids of the LNP formulation is cationic at acidic pH we acidify the solutions initially at pH=7.4 using 0.05%wt of citric acid to reach pH = 4 as we expect an attractive electrostatic interaction between the polarizable lipid and the negatively charged mica surface. However, at pH = 4, we observe a flat layer on the substrate of thickness of the order of 2,3 nm corresponding to a lipid bilayer (Figure 1a and 1b). This

result shows that the LNPs destabilize into lipid bilayers when imaged at pH4 on mica. Furthermore, some particles are completely destabilized while others still present a dome of variable height (between 10 and 20nm) that coexists with the lipid bilayer. These results are consistent with the work of Richter[28], which showed that liposomes tend to destabilize in case of strong interactions with the solid substrate.

To obtain a weak attraction between the LNP and the substrate we use as a substrate a clean glass slide for which we expect the silanol ($Si-OH$) groups to interact through hydrogen bonds with the PEG (CH_2-CH_2-OH) chains of the LNP (see cleaning protocol in the experimental section). In that case, the LNP can be imaged as shown in Figure 1c. We first use a 4 nm tip to obtain a good spatial resolution however such a small tip seems to induce a destabilization of the LNPs during the scan because of the large pressure applied. Indeed Figure 1c shows that two particles indicated with an arrow disappear during the scan as the tip scans the sample from top to bottom. Using a 40 nm tip enables to avoid this destabilization phenomenon and the particles remain stable during the scanning process. We suggest that using a larger tip enables to reduce the pressure applied on the particles for the same applied force as the contact surface between the particle and the tip is larger.

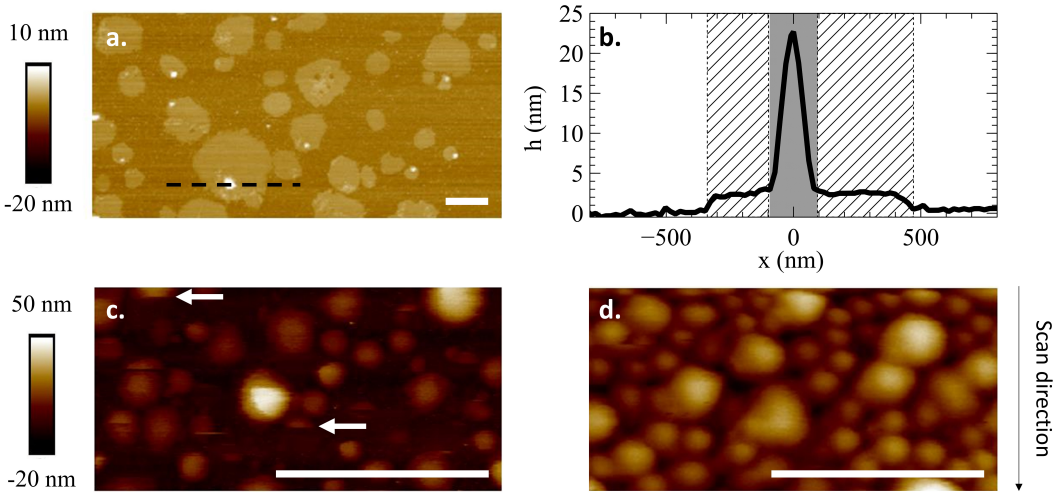

Figure 1: *a- AFM image of a sample of pDNA LNP in citric acid destabilized into a bilayer on a mica surface. The white bar corresponds to 500 nm. The black dots represent the location of the cut. b- profile of the destabilized particles. c-destabilization of the LNPs on a glass surface using a 4 nm tip at pH = 7.4 . d-scan of a layer of LNP and a glass surface with a 40 nm tip at pH = 7.4*

In these conditions, LNPs which are approximately 100 nm in diameter appear flattened

over a height of 40 nm and a diameter of 130 nm because of a competition between their affinity with the surface and the bending rigidity of the phospholipidic membrane[28].

LNPs loaded with mRNA deform more reversibly than the LNPs loaded with pDNA

We first measure approach retract curves for densely packed layers of LNPs loaded with pDNA as shown in Figure 2. The repulsive force between the tip and the particles increases monotonically up to a maximum value of 400 pN (Figure 2a). We choose not to extract a quantitative value of Young modulus or bending rigidity from this approach curve due to the uncertain structure of the LNPs. In previous AFM studies performed on vesicles or capsules the bending rigidity or Young modulus of the membrane was obtained using the Reissner model. However this model relies on hypothesis of small deformations and of membrane thickness being much smaller than the particle diameter. However it is likely not the case for LNP whose structure is still the object of a debate. LNP have been are suggested to either be composed of several aqueous compartments enclosed in .phospholipidic membranes or to present an onion like structure[38]. For this reason we choose to discuss the values of the maximum force reached as well as the reversible character of the deformation.

For h = 40 nm, corresponding to the tip entering in contact with the substrate the measured force suddenly drops to a negative value of the order of 1 nN. The tip then enters in contact with the glass substrate. Upon retraction, the force decreases further and reaches a minimum value of 2 nN. The approach-retraction curves present a large hysteresis due to a strong adhesion force between the tip and the LNP. Such a strong adhesive force is probably due to the capillary force caused by the formation of a liquid meniscus between the tip and the LNP as shown by Barthel et al[41]. These authors used AFM to probe the indentation of a flat lipid bilayer deposited on a solid surface and immerged in water[41]. They found the same order of magnitude for the maximum adhesion force. They suggested that a liquid meniscus composed of phospholipid forms between the tip and the substrate; the adhesion force recorded during the tip retraction is due to the stretching of the meniscus and to the existence of an interfacial tension between the phospholipids and the water. From

the maximum adhesive force, Fadh and knowing the radius of the tip, R, we can estimate the value of the interfacial tension between the lipid and water $\gamma = F_{adh}/2.\pi.R = 15mN/m$. This value has the right order of magnitude for an interfacial tension between apolar liquids and water.

Alternatively Szebeni et al.[38] measured a strong adhesion between the AFM tip and the LNPs and attributed this behaviour to the stretching of biomolecules pulled out off from the LNP with the tip. However we note that in our case the magnitude of the force is five times larger than in their case.

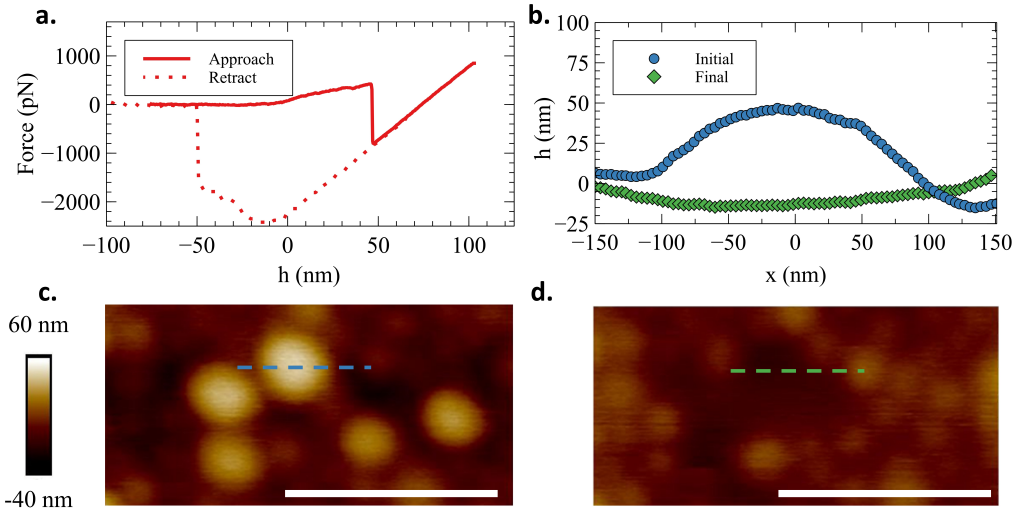

Figure 2: *Mechanical analysis of a pDNA LNP in close packing. (a) Force curve, (b) Section of the particle before and after the force curve, (c) and (d) images of the particle respectively before and after the force curve. Dots represent the location of the cut and the white bar represents a scale of* 200nm.

Comparing the images obtained before and after the mechanical measurement enables to show that the particles are irreversibly destroyed (Figure 2b, c and d). Repeating this test for 20 particles shows that in all of the the cases the particles are irreversibly destroyed. As shown in the schematic drawing of Figure 3a, the particles are constrained laterally by their neighbors which restricts any rearrangement. Therefore the applied pressure may lead to a stretching of the membrane and a subsequent increase of the membrane tension. In the case of stretched phospholipidic membranes increasing the membrane tension is known to cause the nucleation of pores and leak of their content[42–44]. In our case, the stretching of the LNP

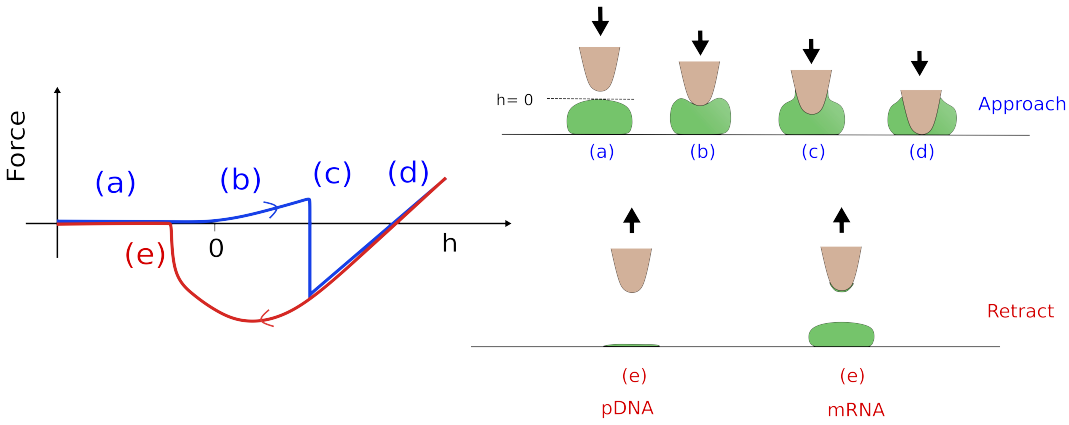

Figure 3: *Schematic summary of the behavior observed during the acquisition of a force curve on pDNA LNP and mRNA LNP. The typical curve of approach and retraction force as a function of piezo position is illustrated. Position h=0 corresponds to the top of the LNP during approach (a). The tip presses against the LNP surface (b). The LNP surface opens and the tip undergoes a sudden attractive force (c), and finally, the tip is in contact with the substrate (d). During the retract, the pDNA breaks and the mRNA can partially recover (e) pDNA and mRNA*

membrane may cause the formation of a pore and enable the penetration of the tip inside the LNP. The irreversible leakage of the LNP content may occur during the retraction of the tip. Hence after the tip retraction the LNP is irreversibly deformed.

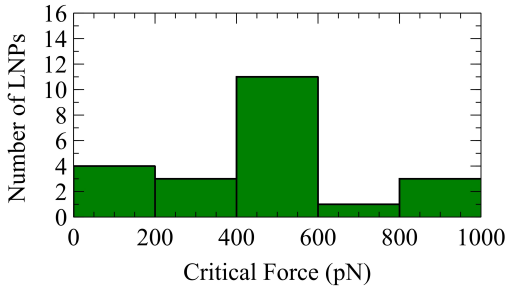

Figure 4: *Histogram of the breaking forces of pDNA LNP in close packing.*

The maximum repulsive force measured before recording the adhesive force is therefore the maximum force that the LNP can sustain before the membrane breaks and the tip penetrates inside the LNP. We plot in Fig.4 the distribution of critical rupture forces obtained for 23 particles. The distribution seems to be centered around $F_{max} = 500$ pN. Some particles burst at zero force and all particles have burst at $F_{max} = 1$ nN.

In the case of LNP loaded with mRNA, the approach-retract curve looks very similar to

the ones obtained with the pDNA LNP. However the imaging of the particles before and after the mechanical measurements leads to different observations from the ones made with the pDNA LNP. Indeed we first measure an increase of the repulsive force and then an adhesion force is measured. The maximum force is of the order of 200 pN (Fig5). Upon retraction of the tip we record a maximum adhesive force of the order of 1500 pN. However unlike for the pDNA, the profile of the mRNA LNP tends to be recovered after the mechanical measurement as can be seen in Fig5 b, c, and d. Indeed in Fig6a we show a statistical analysis of the height ratios of the particles measured before and after the mechanical measurements. For a large fraction of the particles -16 over 23- the height ratio is above 0.6. This contrasts with the pDNA case for which all of the particles were entirely destroyed. Therefore we suggest that eventhough the tip may enter into the mRNA LNP, the LNP may heal at least partially as the tip is removed from the LNP.

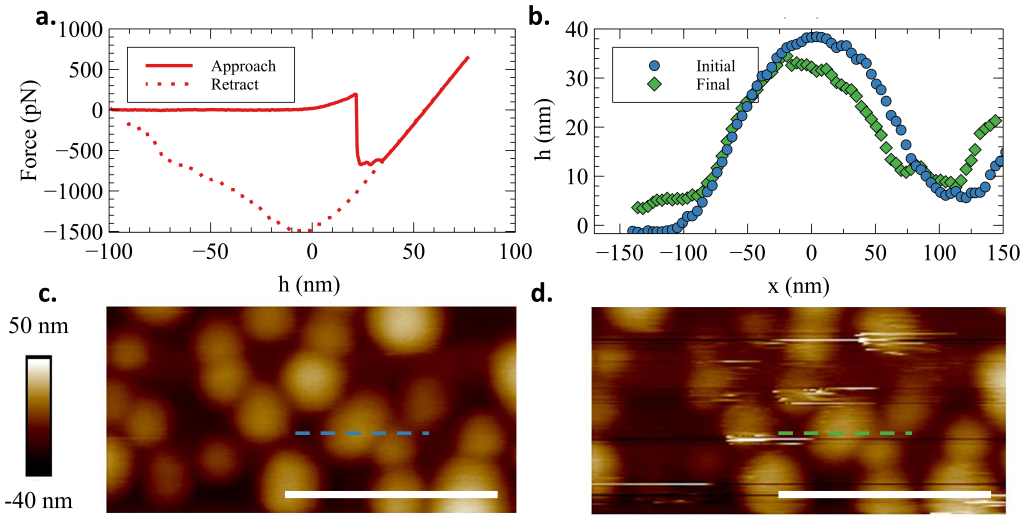

Figure 5: *AFM mechanical measurements obtained with mRNA containing LNPs. a- Force-displacement curves, b- LNP profile before and after a force-distance curve measurement, c- Image of the mRNA LNP before the measurement, and d- after the measurement*

Furthermore we suggest that a small fraction of the LNP content may be extracted and deposited on the tip. Indeed the image that we obtain after the indentation measurement (Figure 5 d) presents some white horizontal segments. This result is obtained each time we image the mRNA particles after an indentation experiment. These white segments are

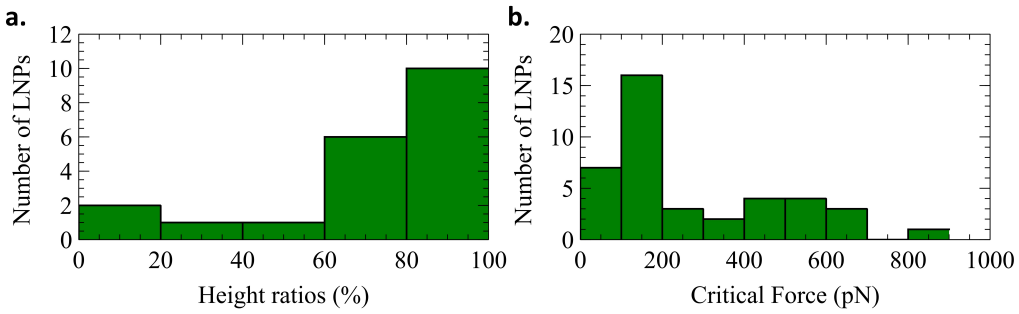

Figure 6: *AFM mechanical measurements obtained with mRNA containing LNPs.a- h ratio (particle height before a mechanical experiment/after a mechanical experiment) for isolated pDNA-LNP. The distribution is obtained over 17 experiments. b- Distribution of maximum force measured with AFM*

probably due to stick/slip events of the tip during the imaging process. Therefore as the tip enters into the mRNA LNP some of the LNP content may contaminate the AFM tip which ultimately disturbs the imaging process that is performed after each indentation.

These results suggest that the mRNA particles deform in a more reversible manner than the pDNA particles. Furthermore, the average maximum force measured for the mRNA LNP is of the order of 200 pN (Fig6 b) while it was 500 pN for pDNA LNP which shows that mRNA LNPs require less force to deform than the pDNA LNP. Hence the mRNA LNP seem softer and to deform more reversibly than the pDNA LNP.

It was recently suggested that pDNA or mRNA establish physical interactions with phospholipids through hydrogen bonds[38]. As pDNA is a more rigid polymer than mRNA we expect that the polyanion/phospholipidic membrane complex is more rigid in the case of pDNA than for mRNA. As a consequence the level of force reached is higher in the case of the pDNA and induces an irreversible destruction of the LNP. At opposite the softer mRNA LNP seem to present a liquid-like behaviour and heal upon retraction of the tip.

Conclusion

We show that it is possible to adsorb LNP using hydrogen bonds between the PEGylated lipid and the silanol present on the glass surface and to subsequently image the LNP using atomic force microscopy. Using a tip with a reduced diameter to obtain a good resolution does not necessarily lead to reliable results as the pressure applied by the tip is larger for a smaller tip for a given applied force and triggers the destabilization of the LNP. We compared force-displacement curves of LNP containing either pDNA or mRNA and found that the results depend on the formulation. LNPs loaded with pDNA present a maximum force of the order of 500 pN above which a strong attraction between the tip and the particles is recorded due to a capillary bridge between the LNP content and the tip. This suggests that the tip enters into the particles. After the retraction of the tip, the pDNA particles are left irreversibly destroyed. For mRNA particles, the maximum force measured is lower and of the order of 150 pN. Despite a strong adhesion between the tip and LNPs that indicates that the tip enters into the particles, the mRNA LNPs remain intact after the retraction of the tip. We suggest that mRNA LNP are softer than the pDNA LNP and that they are able to heal upon tip retraction. The pDNA and mRNA molecules probably complex with the phospholipid membrane hence the behaviour of the membrane probably depends on the stiffness of the biopolymer used. As pDNA is stiffer than mRNA the resulting membrane may be softer and more liquid-like in the case of the mRNA than for pDNA. The level of forces that we record are consistent with the forces recorded with an AFM by Vasir et al during the internalization of nanoparticles by a cells, that range between 20 and 1000 pN[45]. Therefore our study paves the way toward the establishment of the link between particles mechanics and internalization process. This approach may be extended to explore also the phospholipid formulation and manufacturing process which can also impact the nanomechanics of LNPs.

Acknowledgement

We thank Sanofi for providing the LNPs reported in the study, and for the financial support.

References

(1) Akinc, A. et al. A combinatorial library of lipid-like materials for delivery of RNAi therapeutics. *Nature Biotechnology* **2008**, *26*, 561–569.

(2) Aldosari, B. N.; Alfagih, I. M.; Almurshedi, A. S. Lipid nanoparticles as delivery systems for RNA-based vaccines. *Pharmaceutics* **2021**, *13*, 1–29.

(3) Semple, S. C. et al. Rational design of cationic lipids for siRNA delivery. *Nature Biotechnology* **2010**, *28*, 172–176.

(4) Carrasco, M. J.; Alishetty, S.; Alameh, M.-G.; Said, H.; Wright, L.; Paige, M.; Soliman, O.; Weissman, D.; Cleveland IV, T. E.; Grishaev, A.; others Ionization and structural properties of mRNA lipid nanoparticles influence expression in intramuscular and intravascular administration. *Communications biology* **2021**, *4*, 956.

(5) Kiio, T. M.; Park, S. Physical properties of nanoparticles do matter. *Journal of Pharmaceutical Investigation* **2021**, *51*, 35–51.

(6) Genito, C. J.; Batty, C. J.; Bachelder, E. M.; Ainslie, K. M. Considerations for size, surface charge, polymer degradation, co-delivery, and manufacturability in the development of polymeric particle vaccines for infectious diseases. *Advanced nanobiomed research* **2021**, *1*, 2000041.

(7) Wang, M.; Alberti, K.; Sun, S.; Arellano, C. L.; Xu, Q. Combinatorially designed lipid-like nanoparticles for intracellular delivery of cytotoxic protein for cancer therapy. *Angewandte Chemie International Edition* **2014**, *53*, 2893–2898.

(8) Samaridou, E.; Heyes, J.; Lutwyche, P. Lipid nanoparticles for nucleic acid delivery: Current perspectives. *Advanced drug delivery reviews* **2020**, *154*, 37–63.

(9) Chen, D.; Love, K. T.; Chen, Y.; Eltoukhy, A. A.; Kastrup, C.; Sahay, G.; Jeon, A.; Dong, Y.; Whitehead, K. A.; Anderson, D. G. Rapid discovery of potent siRNA-containing lipid nanoparticles enabled by controlled microfluidic formulation. *Journal of the American Chemical Society* **2012**, *134*, 6948–6951.

(10) Li, B.; Luo, X.; Deng, B.; Giancola, J. L. B.; McComb, D. W.; Schmittgen, T. D.; Dong, Y. Effects of local structural transformation of lipid-like compounds on delivery of messenger RNA. *Scientific Reports* **2016**, *6*, 4–11.

(11) Terada, T.; Kulkarni, J. A.; Huynh, A.; Chen, S.; van der Meel, R.; Tam, Y. Y. C.; Cullis, P. R. Characterization of lipid nanoparticles containing ionizable cationic lipids using design-of-experiments approach. *Langmuir* **2021**, *37*, 1120–1128.

(12) Fan, Y.; Marioli, M.; Zhang, K. Analytical characterization of liposomes and other lipid nanoparticles for drug delivery. *Journal of pharmaceutical and biomedical analysis* **2021**, *192*, 113642.

(13) Kulkarni, J. A.; Darjuan, M. M.; Mercer, J. E.; Chen, S.; Van Der Meel, R.; Thewalt, J. L.; Tam, Y. Y. C.; Cullis, P. R. On the formation and morphology of lipid nanoparticles containing ionizable cationic lipids and siRNA. *ACS nano* **2018**, *12*, 4787–4795.

(14) Hassett, K. J. et al. Optimization of Lipid Nanoparticles for Intramuscular Administration of mRNA Vaccines. *Molecular Therapy - Nucleic Acids* **2019**, *15*, 1–11.

(15) Eygeris, Y.; Patel, S.; Jozic, A.; Sahay, G.; Sahay, G. Deconvoluting Lipid Nanoparticle Structure for Messenger RNA Delivery. *Nano Letters* **2020**, *20*, 4543–4549.

(16) Sun, J.; Zhang, L.; Wang, J.; Feng, Q.; Liu, D.; Yin, Q.; Xu, D.; Wei, Y.; Ding, B.; Shi, X.; others Tunable rigidity of (polymeric core)–(lipid shell) nanoparticles for regulated cellular uptake. *Advanced materials* **2015**, *27*, 1402–1407.

(17) Anselmo, A. C.; Mitragotri, S. Impact of particle elasticity on particle-based drug delivery systems. *Advanced drug delivery reviews* **2017**, *108*, 51–67.

(18) Wu, H.; Yu, M.; Miao, Y.; He, S.; Dai, Z.; Song, W.; Liu, Y.; Song, S.; Ahmad, E.; Wang, D.; others Cholesterol-tuned liposomal membrane rigidity directs tumor penetration and anti-tumor effect. *Acta Pharmaceutica Sinica B* **2019**, *9*, 858–870.

(19) Benne, N.; Leboux, R. J.; Glandrup, M.; van Duijn, J.; Lozano Vigario, F.; Neustrup, M. A.; Romeijn, S.; Galli, F.; Kuiper, J.; Jiskoot, W.; Slütter, B. Atomic force microscopy measurements of anionic liposomes reveal the effect of liposomal rigidity on antigen-specific regulatory T cell responses. *Journal of Controlled Release* **2020**, *318*, 246–255.

(20) Kozlovskaya, V.; Dolmat, M.; Kharlampieva, E. Polymeric particulates of controlled rigidity for biomedical applications. *ACS Applied Polymer Materials* **2021**, *3*, 2274–2289.

(21) Preetz, C.; Hauser, A.; Hause, G.; Kramer, A.; Mäder, K. Application of atomic force microscopy and ultrasonic resonator technology on nanoscale: Distinction of nanoemulsions from nanocapsules. *European Journal of Pharmaceutical Sciences* **2010**, *39*, 141–151.

(22) Heurtault, B.; Saulnier, P.; Pech, B.; Benoît, J. P.; Proust, J. E. Interfacial stability of lipid nanocapsules. *Colloids and Surfaces B: Biointerfaces* **2003**, *30*, 225–235.

(23) Yegin, B. A.; Lamprecht, A. Lipid nanocapsule size analysis by hydrodynamic chromatography and photon correlation spectroscopy. *International Journal of Pharmaceutics* **2006**, *320*, 165–170.

(24) Reviakine, I.; Brisson, A. Formation of supported phospholipid bilayers from unilamellar vesicles investigated by atomic force microscopy. *Langmuir* **2000**, *16*, 1806–1815.

(25) Jass, J.; Tjärnhage, T.; Puu, G. From liposomes to supported, planar bilayer structures on hydrophilic and hydrophobic surfaces: An atomic force microscopy study. *Biophysical Journal* **2000**, *79*, 3153–3163.

(26) Kim, J.; Eygeris, Y.; Gupta, M.; Sahay, G. Self-assembled mRNA vaccines. *Advanced Drug Delivery Reviews* **2021**, *170*, 83–112.

(27) Richter, R.; Mukhopadhyay, A.; Brisson, A. Pathways of Lipid Vesicle Deposition on Solid Surfaces: A Combined QCM-D and AFM Study. *Biophysical Journal* **2003**, *85*, 3035–3047.

(28) Richter, R. P.; Brisson, A. Characterization of lipid bilayers and protein assemblies supported on rough surfaces by atomic force microscopy. *Langmuir* **2003**, *19*, 1632–1640.

(29) Takechi-Haraya, Y.; Usui, A.; Izutsu, K.-i.; Abe, Y. Atomic force microscopic imaging of mRNA-lipid nanoparticles in aqueous medium. *Journal of Pharmaceutical Sciences* **2023**, *112*, 648–652.

(30) Dubreuil, F.; Elsner, N.; Fery, A. Elastic properties of polyelectrolyte capsules studied by atomic-force microscopy and RICM. *European Physical Journal E* **2003**, *12*, 215–221.

(31) Ghaemi, A.; Philipp, A.; Bauer, A.; Last, K.; Fery, A.; Gekle, S. Mechanical behaviour of micro-capsules and their rupture under compression. *Chemical Engineering Science* **2016**, *142*, 236–243.

(32) Sarrazin, B.; Tsapis, N.; Mousnier, L.; Taulier, N.; Urbach, W.; Guenoun, P. AFM investigation of liquid-filled polymer microcapsules elasticity. *Langmuir* **2016**, *32*, 4610–4618.

(33) Neubauer, M. P.; Poehlmann, M.; Fery, A. Microcapsule mechanics: From stability to function. *Advances in Colloid and Interface Science* **2014**, *207*, 65–80.

(34) Delorme, N.; Fery, A. Direct method to study membrane rigidity of small vesicles based on atomic force microscope force spectroscopy. *Physical Review E - Statistical, Nonlinear, and Soft Matter Physics* **2006**, *74*, 3–5.

(35) Delorme, N.; Bardeau, J. F.; Carrière, D.; Dubois, M.; Gourbil, A.; Mohwald, H.; Zemb, T.; Fery, A. Experimental evidence of the electrostatic contribution to the bending rigidity of charged membranes. *Journal of Physical Chemistry B* **2007**, *111*, 2503–2505.

(36) Vorselen, D.; Marchetti, M.; López-Iglesias, C.; Peters, P. J.; Roos, W. H.; Wuite, G. J. Multilamellar nanovesicles show distinct mechanical properties depending on their degree of lamellarity. *Nanoscale* **2018**, *10*, 5318–5324.

(37) Forchette, L.; Sebastian, W.; Liu, T. A comprehensive review of COVID-19 virology, vaccines, variants, and therapeutics. *Current medical science* **2021**, 1–15.

(38) Szebeni, J.; Kiss, B.; Bozó, T.; Turjeman, K.; Levi-Kalisman, Y.; Barenholz, Y.; Kellermayer, M. Insights into the Structure of Comirnaty Covid-19 Vaccine: A Theory on Soft, Partially Bilayer-Covered Nanoparticles with Hydrogen Bond-Stabilized mRNA–Lipid Complexes. *ACS nano* **2023**, *17*, 13147–13157.

(39) Ripoll, M.; Martin, E.; Enot, M.; Robbe, O.; Rapisarda, C.; Nicolai, M.-C.; Deliot, A.; Tabeling, P.; Authelin, J.-R.; Nakach, M.; others Optimal self-assembly of lipid nanoparticles (LNP) in a ring micromixer. *Scientific Reports* **2022**, *12*, 9483.

(40) Sabnis, S.; Kumarasinghe, E. S.; Salerno, T.; Mihai, C.; Ketova, T.; Senn, J. J.; Lynn, A.; Bulychev, A.; McFadyen, I.; Chan, J.; others A novel amino lipid series for mRNA delivery: improved endosomal escape and sustained pharmacology and safety in non-human primates. *Molecular Therapy* **2018**, *26*, 1509–1519.

(41) Barthel, E.; Lin, X. Y.; Loubet, J.-L. Adhesion energy measurements in the presence of adsorbed liquid using a rigid surface force apparatus. *Journal of colloid and interface science* **1996**, *177*, 401–406.

(42) Chabanon, M.; Ho, J. C.; Liedberg, B.; Parikh, A. N.; Rangamani, P. Pulsatile lipid vesicles under osmotic stress. *Biophysical journal* **2017**, *112*, 1682–1691.

(43) Sandre, O.; Moreaux, L.; Brochard-Wyart, F. Dynamics of transient pores in stretched vesicles. *Proceedings of the National Academy of Sciences* **1999**, *96*, 10591–10596.

(44) Idiart, M. A.; Levin, Y. Rupture of a liposomal vesicle. *Physical Review E* **2004**, *69*, 061922.

(45) Vasir, J. K.; Labhasetwar, V. Quantification of the force of nanoparticle-cell membrane interactions and its influence on intracellular trafficking of nanoparticles. *Biomaterials* **2008**, *29*, 4244–4252.